Performance assessment of reinforced concrete after long-term exposure to a marine environment

Jaehwan Kim

W. John McCarter*

Benny Suryanto

School of Energy, Geoscience, Infrastructure and Society,

Institute for Infrastructure and Environment,

Heriot-Watt University,

Edinburgh, EH14 4AS,

United Kingdom,

W. John McCarter: ORCID: 0000-0002-1949-2856

Benny Suryanto: ORCID: 0000-0002-3979-9994

* Corresponding Author

E-mail: w.j.mccarter@hw.ac.uk

Tel: +44 (0)131 451 3318

ABSTRACT

The performance of CEM I, CEM III/A and CEM II/B-V reinforced concrete slabs which have been exposed to a marine environment for 18 years is presented. Performance is assessed in terms of porosity, degree of saturation, chloride concentration and electrical resistivity gradients evaluated through the surface ~150mm; the condition of the embedded steel was evaluated using electrochemical techniques. Based on the parameters related to chloride transport, two new environmental factors were introduced into the ClinConc model to predict chloride ingress into unsaturated concrete. A monitoring system is also presented enabling remote interrogation of those slabs located at the marine exposure site.

Keywords: Field concrete; Chloride-induced corrosion; Electrical resistivity; Electrochemical measurements; ClinConc model; Long-term behaviour

1. Introduction

Deterioration of reinforced concrete structures caused by corrosion of the embedded steel is a major problem faced by the construction industry, with chloride-induced corrosion being the most commonly reported mechanism affecting concrete durability [1]. Chloride ions come from deicing salt used on roads during the winter months (XD1, XD2 and XD3 environments according to BS EN 206 [2]) or from the marine environment where, for example, bridges span tidal estuaries (XS1, XS2 and XS3 environments according to BS EN 206). As it is the concrete cover-zone (i.e. the surface 50mm or so) which protects the reinforcing steel from the external environment, it has a major influence on the durability of reinforced concrete by providing the only barrier to chloride ingress. The protective qualities of cover-zone concrete are thus of considerable interest to engineers as the service-life of a structure depends, to a large extent, on the permeation properties of the cover-zone concrete which, in turn, will be influenced by the cementitious binder.

To ensure the protective quality of the cover-zone, the majority of the current design codes deal with this aspect on the basis of a prescriptive approach by specifying limiting parameters such as minimum strength grade, minimum binder content and maximum water-binder ratio (w/b) for a series of well-defined environmental classes. With regards to the marine environment and chloride induced corrosion, there are, generally, three exposure classes with the tidal/splash zone considered to be the most vulnerable. Table. 1 presents typical values from a number of design codes for structures subjected to this particular exposure condition. The maximum w/b ratio is ~0.4, while the required minimum binder content, compressive strength and maximum chloride content vary from one specification to another, most likely driven by differences in local materials, practices and exposure conditions. As these factors are highly variable and strongly dependent on local conditions, it would be difficult to

recommend limiting values which would ensure adequate durability performance throughout the life of a structure. Satisfactory guidelines for ensuring adequate reinforced concrete durability can only be developed by evaluating concrete performance under a range of field exposure conditions over an extended period of time. Only then can there be a move from prescriptive durability specifications to performance-based methods [3].

Design Code	Maximum w/b	Minimum binder content (kg/m^3)	Minimum f_c (MPa)	Maximum chloride content (% weight of cement)	Country	Reference
EN 206:2013 +A1: 2016	0.45	340	35	0.4	EU	[2]
BS 8500-1:2015 + A1:2016*	0.35-0.55	320-380	25-40	0.3	UK	[4]
ACI 318-14	0.4	+	35	0.15**	USA	[5]
CSA A23.1-09	0.4	+	35	+	Canada	[6]
JGC15/16 SSMC–2007	0.45	330# 300##	+	1.2kg/m3###	Japan	[7,8]

Note: f_c compressive strength; * Intended working life of at least 100 years; ** water soluble chloride content; # maximum aggregate size 20 or 25mm; ## maximum aggregate size 40mm; ### total chloride content per unit volume of concrete.

Table 1 Limiting values of mix design in the codes for marine structures subjected to tidal and splash zone.

Regarding durability design, there is a recent growing interest to move away from the prescriptive method towards the performance-based approach. For example, whilst BS EN 206 [2] still stipulates prescriptive-based approach for durability, Section 5.3.3 of this code allows for performance-related methods and defines concrete on the basis of an *equivalent*

durability procedure (EDP); however, in order to fully implement a performance-based strategy requires:

(1) long-term experience of local materials and practices, and a detailed knowledge of the local environment;
(2) test methods based on approved and proven tests that are representative of actual conditions and have approved performance criteria; and,
(3) analytical models that have been calibrated against test-data representative of actual conditions in practice.

Supplementary cementitious materials (SCMs) such as fly ash (FA) and ground granulated blast-furnace slag (GGBS) have been extensively used to replace Portland cement (PC) in concreting operations. It is well-known that these materials are beneficial in resisting chloride transport through their reduced permeability and high chloride binding capacity [9–12] although the chloride threshold level (CTL) regarding these materials is still controversial [13-16]. Moreover, according to BS 8500-1 [4], the use of SCMs is recommended in chloride environments although specification of such concretes still relies on prescriptive methods rather than a performance-based approach. For example, a reinforced concrete element with an intended working life of at least 100 years exposed to XS3 environment, the use of CEM I (Portland cement clinker) concrete is now not recommended [4], whereas CEM III/A (blast furnace cement) concrete or CEM II/B-V (fly ash cement) concrete require a minimum cover to steel of 60mm, plus an allowance in design for deviation. Additionally, maximum w/b and minimum compressive strength are also defined in the specification although these parameters cannot fully ensure the performance of concrete in chloride-rich environments. In comparison to laboratory testing, there is a dearth of long-term, field data for chloride-exposed concrete (see requirements in (1) - (3) above) which has resulted in a slow uptake of a performance-based approach for concrete specification.

In the current study, a comprehensive assessment of the performance of 18 year old reinforced concrete slabs subjected to XS3 environment is presented (i.e. concrete in the tidal and splash zone). The testing program included evaluating the chloride concentration, porosity, degree of saturation and electrical resistivity at discrete points within the surface ~150mm. Regarding the condition of the steel surface, half-cell potential, polarisation resistance and *B*-value were measured therefore providing long-term data on the performance of steel in concrete. Furthermore, the ClinConc model [17] was combined with two new environmental factors to predict the time to corrosion initiation for the field concrete slabs.

2. Field durability studies

To date, a number of marine exposure sites have been installed in various countries around the world in an attempt to assess the performance of concrete over an extended period of time. For example, Tang and Utgenannt [18] exposed more than 40 concrete samples to a marine environment on the west coast of Sweden; after 13-years of exposure, it was suggested that oxygen availability plays an important role in corrosion initiation and that a total chloride content of 1% by weight of binder can be regarded as the critical value for significant corrosion to occur. Using the Building Research Establishment (BRE) exposure site on the Thames Estuary in South-East England, Thomas et al. [19] reported that chloride threshold levels for Portland cement concrete containing fly-ash decreases with increasing fly-ash replacement. The chloride concentration was measured using an X-ray fluorescence technique and the condition of the embedded steel bars was evaluated using a weight loss method. After 4-years exposure, it was found that the total chloride threshold levels were 0.7%, 0.65%, 0.5% and 0.2% by weight of binder, corresponding to concrete with fly-ash replacement levels of 0%, 15%, 30% and 50%, respectively. It was also found that the diffusion coefficient decreases with increasing fly-ash replacement and this exerts a greater influence on corrosion rate than the effect of decreasing chloride threshold level with

increasing fly-ash content. Otieno et al. [20] carried out parallel investigations on both uncracked and pre-cracked concretes (containing SCM's) exposed to accelerated laboratory testing and a natural marine environment at Table Bay in Cape Town (exposure time was 2.25 years). Using coulostatic and half-cell potential techniques, they found that the corrosion rate increased with crack width and decreased with concrete quality and cover-depth. The use of SCMs was found to result in significant reductions in corrosion rate regardless the exposure condition studied. The corrosion process under the accelerated condition was found to be different to that under the natural environment. Thomas et al. [21] demonstrated that concrete with high levels of GGBS replacement displays a satisfactory performance even though being exposed to a highly aggressive marine environment for 25 years at Treat Island in the USA. However, it was recommended that the w/b ratio must be kept low, ideally ≤0.4. Overall, these studies highlight the importance of field studies to understand the durability performance of different concretes under a particular exposure condition.

Considering the complexity of natural exposure, it would be desirable to express the durability of concrete exposed to marine environments by a single factor with electrical resistivity being increasingly attractive for *indexing* durability. Regarding the latter, this testing methodology has been utilized by McCarter et al. [22] in a sensor system to study both the short- and long-term response of the cover-zone concrete subjected to a range of marine exposure conditions. It was shown that the properties of concrete change with time and depth due to further hydration and are affected by ionic ingress. Based on chloride profiling data and electrochemical measurements on concrete exposed to marine environment, Morris et al. [23] proposed a relation between electrical resistivity of concrete and chloride threshold level and highlighted that the resistivity of concrete can be regarded as an effective parameter to evaluate the risk of chloride-induced corrosion. To establish the

149 relationship between performance of the field concrete and electrical resistivity, additional
150 studies are clearly still required.
151

152 **3. Experimental**

153 *3.1. Field conditions and slab details*

154 The concrete slabs used in this study had been exposed to three different marine
155 environments specified in BS EN 206 [2] and BS 8500-1 [4]
156 (1) above the high-water level in the atmospheric spray zone (XS1);
157 (2) the tidal and splash zone (XS3); and,
158 (3) below mid-tide level (XS2 environment).
159

160 The slabs were positioned at a marine exposure site on the Dornoch Firth in north-east
161 Scotland (see Fig. 1) in 1998.

162

163 Fig. 1. Location of marine exposure site.

The concrete mixes used in the marine exposure program are presented in Table 2 [24]. The slabs were 300×300×200(thick)mm cast in plywood formwork which had been given a coat of proprietary release agent prior to casting. After casting, the slabs were compacted into two layers on a vibrating table and demoulded after 24-h. On demoulding, the slabs were then wrapped in damp hessian and covered with polyethylene sheeting under a sheltered condition for 7-days and all sides and the top face of the slabs were then coated with several coats of a high-build epoxy-based paint to ensure one-dimensional movement of water/moisture (see Figs. 2(a)-(c)). The slabs contained two Ø16mm×200mm ribbed rebar sections which had been cleaned and degreased prior to installation; they were positioned to have a 50mm cover from the working face and sides. A Ø6mm×200mm stainless steel (s/s) bar was positioned centrally between these two rebars (see Fig. 2(b)). All bars had electrical connections and the cut ends of the rebars were coated with epoxy glue. The rebar and s/s rod formed a working-electrode/counter-electrode system and, when used in conjunction with a surface mounted reference electrode, facilitated rebar corrosion measurements viz. half-cell and linear polarisation.

Mix designation	CEM I (kg/m^3)	GGBS (kg/m^3)	FA (kg/m^3)	Coarse aggregate		Fine aggregate (kg/m^3)	WR* (l/m^3)	w/b	f_{28}** (MPa)
				20 mm (kg/m^3)	10 mm (kg/m^3)				
CEM I (PC)	460	+	+	700	350	700	1.84	0.4	70 (64.9)
CEM III/A (GGBS/40)	270	180	+	700	375	745	3.60	0.44	53 (53.9)
CEM II/B-V (FA/30)	370	+	160	695	345	635	2.65	0.39	58 (49.0)

*WR water reducer; ** f_{28} 28-day compressive strength. Figure in brackets represents compressive strength for migration test samples.

Table 2 Mix design used in field slabs [24].

For monitoring the electrical resistance within the cover zone concrete, seven pairs of stainless-steel pin-electrodes were mounted on a PVC former to form an electrode array [25]

which was, subsequently, embedded within each slab at the time of casting (see Fig. 2(a)). This allowed resistance measurements to be obtained at discrete depths from the exposed working surface i.e. 5, 10, 15, 20, 30, 40 and 50 mm. For each pair of electrodes, the spacing between the individual pins was 10mm. Four thermistors were also mounted on the PVC former enabling temperature measurements to be obtained at 10, 20, 30 and 40 mm from the working surface. Colour-coded cables were connected to the electrodes, thermistor, s/s bar and rebars and then were taken into a watertight glass-reinforced plastic (GRP) enclosure placed in the face opposite to the working face (see Fig. 2(c)); a 37-pin, multi-pole female D connector was used to terminate all wires.

Within approximately 5-weeks after demoulding, the slabs were transported to the marine site and were placed to the site. The 300×300mm face cast against the plywood formwork was used as the *working face* and positioned vertically facing the sea; six slabs per mix were secured within galvanised steel frames and positioned at each exposure condition (see Fig. 3). In XS2 and XS3, three slabs (one for each mix) were hard-wired (see Fig. 4(a)) to a control-box facility to interrogate/monitor the slabs remotely (see Fig. 4(b) and (c)).

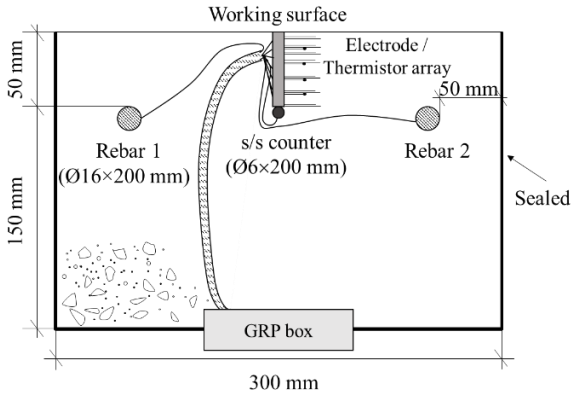

(a)

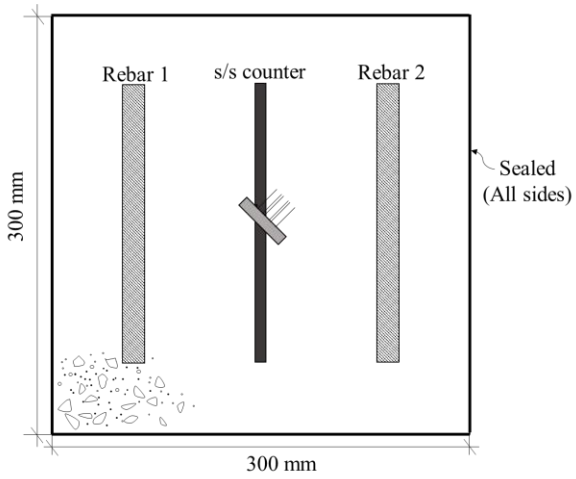

(b)

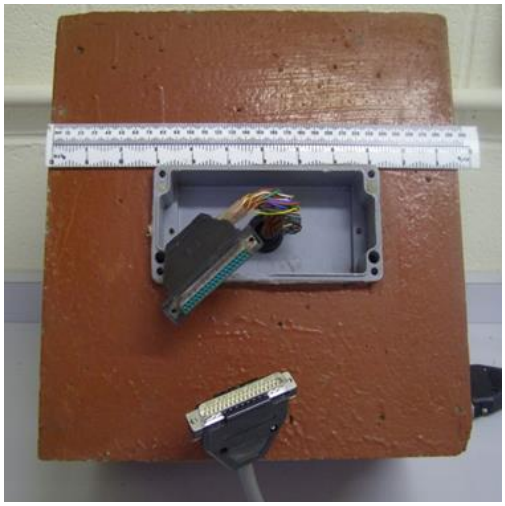

(c)

Fig. 2. Concrete slab used in the experimental program showing (a) sectional view, (b) plan view and (c) GRP box enclosing a 37-pin D connector and lead.

Fig. 3. Frames containing slabs installed at Dornoch field site in XS1, XS2 and XS3 positions.

211

212

213

214 (a)

215

216 (b)

217

218

219

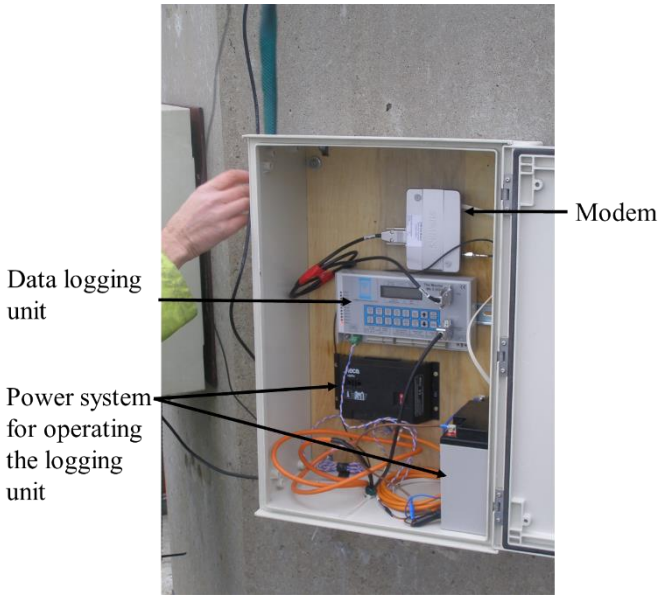

(c)

Fig. 4. (a) Concrete slabs hard-wired for remote interrogation in XS3 environment (b) watertight enclosure for monitoring equipment and (c) modem, data logging unit and power source for the monitoring system.

In this study, only those slabs exposed to an XS3 environment were returned to the laboratory as it is in the tidal and splash zones where reinforced concrete is highly susceptible to chloride-induced corrosion [4]. After 18 years exposure, three slabs, one for each mix (see Fig. 5), were retrieved and double-sealed with polythene *film* to preserve the moisture condition of samples. A series of experiments and sampling was then conducted in a laboratory environment when the slabs had equilibrated at laboratory temperature (20±1ºC).

238 Fig. 5. Concrete slabs retrieved from frame in XS3 environment.

239 *3.2 Tests relating to chloride transport*

240 In relation to the chloride transport behaviour of concrete, the following key performance
241 indicators were obtained from the slabs, (1) degree of saturation, (2) porosity, and (3)
242 chloride concentration. With reference to Fig. 6(a), for degree of saturation and porosity
243 measurements the slab was cut vertically on sections A-A' and B-B' to give a
244 300×200×50(thick)mm 'slice' of concrete (Fig. 6(b)); seven prismatic samples
245 50×50×20(thick)mm were then cut from the central portion of this slice as depicted in Figs.
246 6(b) and (c). To minimise any changes in the moisture state of the concrete, cutting was
247 carried out using a diamond-concrete saw without water cooling. After cutting, the mass of
248 each prism was immediately measured. To minimise any potential damage in microstructure
249 due to micro-cracking at elevated temperatures, a low drying temperature was chosen with
250 the samples dried to constant mass in an oven at 50±2ºC. The samples were then vacuum
251 saturated with distilled water under a pressure of 30mbar which was maintained for 4 hours.
252 During the saturation stage, the mass of each sample was periodically measured using a scale
253 of ± 0.01g accuracy until equilibrium was achieved at which time the following criterion was
254 satisfied:

255 $$\left|\frac{m(t_i)-m(t_{i+1})}{m(t_{i+1})}\right| \times 100 \leq 0.1(\%) \quad (1)$$

where $m(t_i)$ is the mass measured at time t_i and $m(t_{i+1})$ is the mass measured after time t_{i+1}. The degree of saturation and porosity were then calculated as follows:

$$S_r\ (\%) = \frac{(m_o - m_d)}{(m_v - m_d)} \times 100 \quad (2)$$

$$\varphi\ (\%) = \frac{(m_v - m_d)}{(V_s \times \gamma_w)} \times 100 \quad (3)$$

where S_r is degree of saturation (%), m_o is the original sample mass (g), m_d is the dried sample mass (g), m_v is the vacuum saturated sample mass (g), φ is porosity (%), γ_w is the density of distilled water (=1 g/cm^3), and V_s is the sample volume (cm^3).

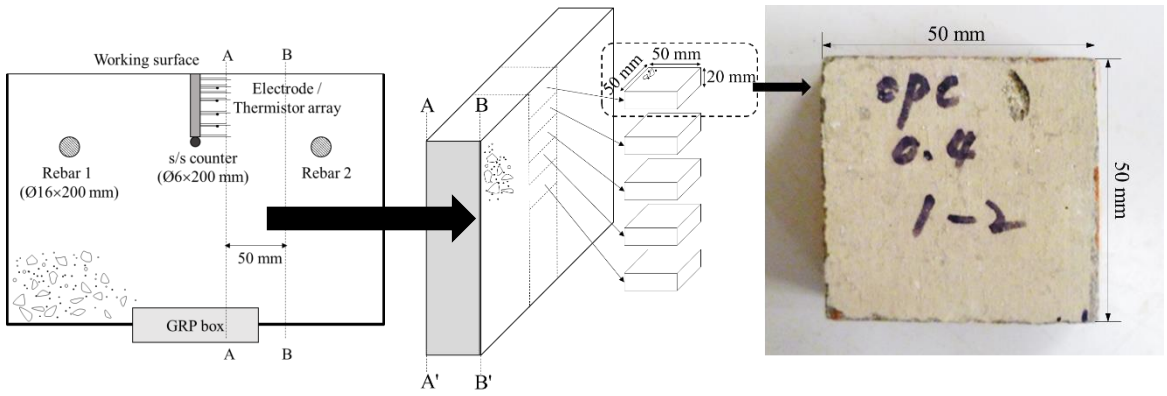

(a) (b) (c)

Fig. 6. (a) Schematic of concrete slab showing cutting on sections A-A' and B-B', (b) cutting procedure for concrete 'slice', and (c) cut prisms used for evaluating porosity, degree of saturation and electrical resistivity.

The 300mm×200mm exposed surface (A-A/A'-A' on Figs. 7(a) and (b)) of each slab was used to obtain dust samples for chloride profiling. Dust samples were obtained using a hammer-action drill with an 8-mm diameter drill bit. The depth of investigation for all concretes covered the surface 0- ~100 mm using 8-mm depth increments (see Fig. 7(b)) between drill

holes. Several sampling locations (6–8 at each depth, see Fig. 7(c)) were drilled to a depth of 30mm depth and powder taken to be representative of bulk concrete. The powder was then sieved using a 125μm sieve with at least 10g of powder collected at every depth increment. The total chloride (acid soluble) concentration in ppm at each depth was measured using Chloride QuanTab® strips (manufactured by HACH). The concentration was then converted to chloride concentration in % weight of binder. From the chloride profile, the apparent diffusion coefficient and surface chloride concentration were calculated by fitting the error function solution to Fick's 2nd law. The pre-existing chloride concentration in the concrete mixes (C_o) was negligible, hence,

$$C(x,t) = C_s\left(1 - erf\left(\frac{x}{2\sqrt{D_a \cdot t}}\right)\right) \quad (4)$$

where $C(x,t)$ is the total chloride concentration (%) at depth of x (m) from the surface at exposure time, t (sec), C_s is the surface chloride concentration (%), D_a is the apparent diffusion coefficient (m^2/s).

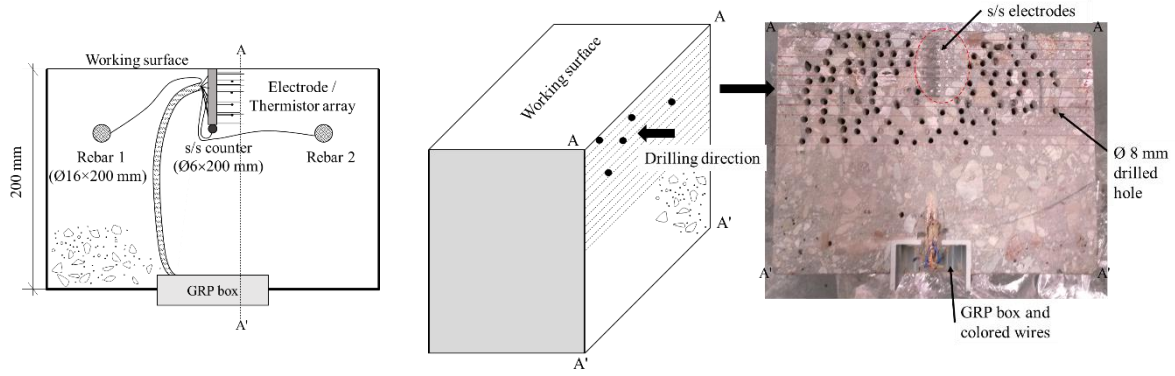

(a) (b) (c)

Fig. 7. Sampling procedure for measuring chloride concentration, (a) cut surface A-A/A'-A', (b) drilling direction parallel to exposed surface, and (c) at a particular depth, powder was collected from 6-8 drill-holes.

291 The migration coefficient is widely used as a performance indicator to evaluate the resistance
292 of chloride transport, particularly in European countries [26]; in addition, the 6-month
293 migration coefficient is required in the implementation of the ClinConc model. Samples for
294 the migration test were cast at a later stage using a similar mix specification to that used in
295 the 18 year old concrete slabs (see Table 2) thereby conforming to the reference concrete
296 defined in the equivalent durability procedure in Section 6.2 of PD CEN/TR 16563:2013 [26];
297 28-day compressive strength tests were also carried out using 100 mm cubes. For migration
298 testing, Ø100mm×300mm cylinders were cast in PVC moulds; 24-h after casting, the
299 cylinders were placed in curing tank. After 6-months curing, three concrete disks were
300 extracted from the middle of the cylinders using a diamond saw and the migration coefficient
301 was determined following the test procedure specified in NT Build 492 [27]. The average
302 compressive strength and migration coefficient of the reference concrete are summarised in
303 Tables 2 and 6, respectively.

304 *3.3. Tests relating to corrosion of steel*

305 Prior to the tests detailed above, the condition of the embedded steel bars was investigated
306 using the half-cell potential technique, galvanostatic pulse technique and the Tafel
307 extrapolation technique. A three-electrode configuration was used with the two mild steel
308 rebars as individual working electrodes, the stainless-steel rod as a counter electrode and a
309 surface-mounted copper-copper sulphate reference electrode (CSE). A Solartron 1287
310 Electrochemical Interface was used and controlled by CorrWare® software. The corrosion
311 potential was determined when the potential changed by <10 mV/s. The exposed area of each
312 working electrode was 100.53 cm^2. Between galvanostatic pulse measurement and Tafel
313 extrapolation measurement, a depolarisation time of 10 minutes was maintained to recover
314 the corrosion potential. For the galvanostatic pulse technique, a constant current of 25μA

corresponding to an average current density of 0.25μA/cm^2 was applied to the working electrode for 10s. From the result, the ohmic resistance and polarisation resistance were estimated using a modified Randles circuit combined with an exponent as shown in Eq. (5) [28],

$$V_t(t) = I_{app}R_\Omega + I_{app}R_p\left[1 - \mathrm{e}^{-\left(\frac{t}{\tau}\right)^\beta}\right] \quad (5)$$

where $V_t(t)$ is the potential of the steel bar with measuring time t; I_{app} is the applied current; R_p is the polarisation resistance; R_Ω is the ohmic resistance; τ is the time constant ($= R_pC_{dl}$); β is the non-ideality exponent ($0< \beta \leq 1$); and C_{dl} is the double-layer capacitance.

To evaluate the *B*-value, a Tafel extrapolation test was also carried out. The sweep range was from –300mV to +600mV versus the free corrosion potential and the scan rate was 10mV/min. The curve corresponding to ±200mV around the corrosion potential was fitted using a commercial program (CView Version 3.5a.). The *B*-value was calculated with the Tafel constants obtained from the fitting as follows:

$$B = \frac{\beta_a\beta_c}{2.3\,(\beta_a+\beta_c)} \quad (6)$$

where β_a and β_c are Tafel constants from the anodic branch and the cathodic branch, respectively (mV/dec).

3.4 Electrical resistivity of concrete

The electrical resistivity of the concrete was evaluated for two test conditions (a) the field slabs which were returned to the laboratory, and (b) their counterparts positioned at the XS3 environment at the marine exposure site. For (a), the electrical resistance of the vacuum-

saturated 50×50×20mm prisms used in the porosity and saturation tests was measured using a LCR meter (Agilent 4263B) at a frequency of 1kHz and signal amplitude of 350mV. A two-electrode technique was employed with intimate contact between the electrodes and prism obtained using synthetic sponges which had been saturated with $Ca(OH)_2$ solution. The resistance was then converted to resistivity by Eq. (7),

$$\rho = \frac{A}{L} R_c \tag{7}$$

where ρ is the resistivity of the concrete (Ω·m), A is the cross-sectional area of the sample (= 0.025m^2), L is the sample thickness (= 0.02m) and R_c is the measured concrete resistance (Ω).

For condition (b), the electrode and thermistor array described above was used to obtain discretized resistance and temperature measurements using the remote interrogation system. Data were uploaded through a dial-up modem and then recorded in a CSV file using a software installed in the office-based computer. A measurement cycle was carried out every 6-hours for approximately 1 month (September/October). The resistance measured by the thermistor was converted to *degree Celsius using* the Steinhart-Hart equation:

$$T = [A + BlnR + C(lnR)^3]^{-1} - 273.15 \tag{8}$$

where R is the measured thermistor resistance (Ω); T is temperature (ºC); and A, B, and C are coefficients depending on the type of thermistor which were, 1.29×10^{-3}, 2.36×10^{-4} and 9.51×10^{-8} K^{-1}, respectively [29].

Prior to embedding the electrode array in the slabs, the electrode arrangement was calibrated in solutions of known resistivity thereby enabling the measured resistance of concrete, between the electrodes, R_c (Ω), to be converted to resistivity, ρ (Ω·m) through Eq. (9):

$$\rho = kR_c \tag{9}$$

where *k* is the calibration factor for the electrode geometry which was obtained as 0.0125m ± 5%. The resistivity of the calibrating solutions covered the anticipated range of concrete resistivity (i.e. 10–100Ωm).

4. Results and discussion

4.1 Performance Indicators for Chloride Transport

4.1.1 Porosity Gradient

Dissolved chlorides move through the connected pore network in concrete and, when the chloride concentration at the steel surface exceeds a certain critical value (the chloride threshold level CTL), depassivation will occur and corrosion will be initiated. Before depassivation, however, the capillary pore structure within the cementitious binder is a key factor in determining chloride transport behaviour in concrete and porosity is an important performance parameter in this respect. Fig. 8 presents the porosity gradient for each concrete slab through the surface 140mm with the average porosity given in the Figure legend. Interestingly, the porosity increases with type of binder in the order: CEM I (10.3%) < CEM III/A (10.9%) < CEM II/B-V (12.5%). From the results, it is evident that concretes containing SCMs have a slightly higher porosity than the plain Portland cement (CEM I) concrete; however, it is well-established that concretes containing SCMs have a higher resistance to chloride transport than plain Portland cement concretes [10]. In attempting to explain this anomaly, the various types of pores that exist in concrete are shown schematically in Fig. 9 [30]. It could be deduced that whilst the overall porosity of the concretes containing SCMs is higher than plain CEM I concrete, the capillary pore network within these concretes will be more tortuous and disconnected in comparison to the CEM I concrete. This would be in agreement with previous studies [31, 32]. The result of this would imply that the rate of

chloride transport would be slower in these concretes and that porosity, itself, cannot be used solely as an indicator of concrete performance without due consideration of pore type as depicted in Fig. 9.

Although porosity varied with depth due to heterogeneity of the concrete (see Fig. 8), the variation is considered small. It is noteworthy that the porosity of the surface 0-20mm was generally lower than those at other depths. This could be explained, in part, by chloride binding effects which can constrict capillary pores and reduce porosity.

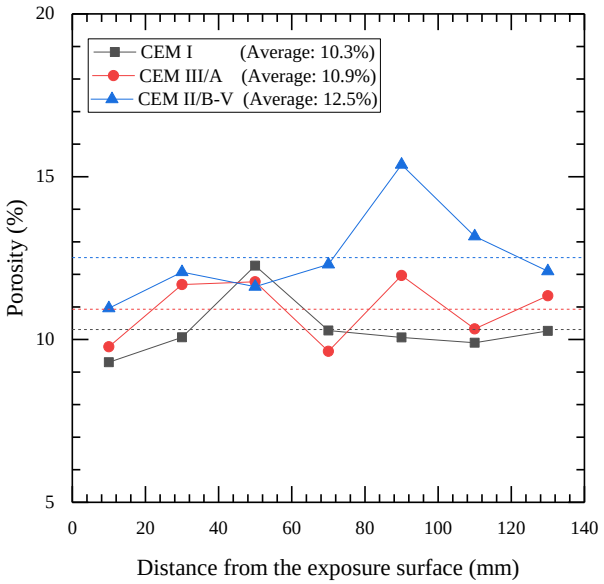

Fig. 8. Porosity gradient of 18-year old concrete through the surface 140mm (XS3 environment).

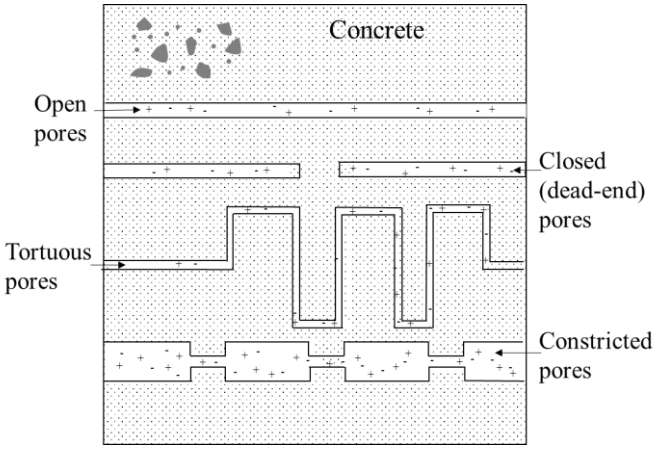

Fig. 9. Schematic representation of different types of capillary pore in concrete.

4.1.2 Degree of Saturation

As (free) chlorides dissolved in the pore-water are only mobile through the continuous water-filled capillary pores, chloride transport will be significantly influenced by the moisture state of the concrete. At low moisture-contents corresponding to a value which is higher than the critical moisture content below which capillary absorption becomes dominant, less chloride will be transferred through the pore solution assuming that there are no external forces for chloride transport. Until now, it is noted that there is no evident boundary value between capillary suction and diffusion with respect to chloride transport in concrete. From Fig. 10, the degree of saturation was shown to be in the order: CEM I (83%) > CEM III/A (73%) > CEM II/B-V (67%) and is the reverse of the order in porosity. This could be explained as the CEM I concrete will have a more connected porosity hence allow a more rapid ingress of water. At 10mm depth, the degree of saturation was, generally, higher than at other depths as it is this region which is more susceptible to the wet/dry cyclic regime and represents the convective zone. It could be inferred that the degree of saturation of the concrete at depths >10mm remains relatively stable at this exposure environment. In other words, chloride transport rate in the tidal zone is lower than that in the submerged zone as the convective zone in tidal zone is negligible (~5mm) [33] and the concrete is not continuously exposed to

chlorides. This result is in agreement with a previous study [34]. The degree of saturation must be considered when the chloride transport rate is determined and represents an important performance indicator in this respect.

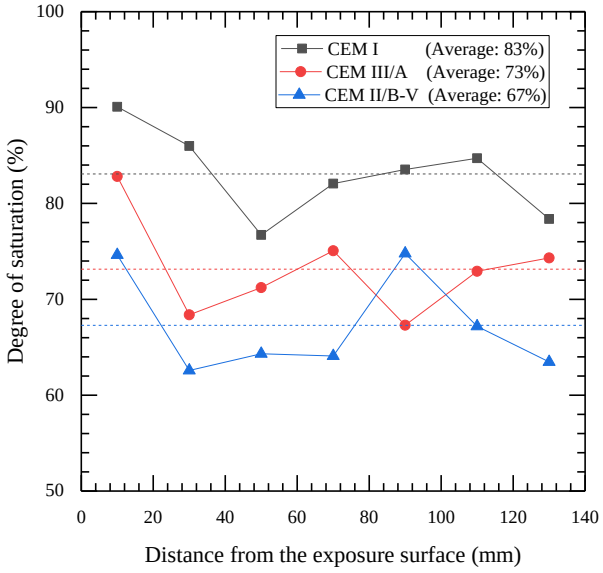

Fig. 10. The variation in the degree of saturation of 18-year old concrete through the surface 140mm (XS3 environment).

4.1.3 Chloride Ingress

The chloride profiles for each concrete (one slab per mix) after 18 years exposure are presented in Fig. 11. As expected, the CEM I concrete has a higher concentration of chlorides at all depths in comparison to the other concretes. Curve-fitting using Eq. (4), obtained diffusion coefficients, D_a, of 1.39×10^{-12} m^2/s, $4.21\times10^{-13}m^2/s$, and $4.21\times10^{-13}m^2/s$ for CEM I, CEM III/A and CEM II/B-V concrete, respectively, and surface chloride concentrations, C_s, of 4.54%, 4.46% and 5.56% (by weight of binder), respectively. Direct comparison with previous studies is difficult as the concretes had different mix compositions and were exposed to different curing and exposure conditions [10, 35]. However, it is clear that SCM concretes were observed to be beneficial in resisting chloride transport, particularly at depths >20mm.

Regarding chloride-induced corrosion, the chloride concentration at the surface of the steel is a critical factor in corrosion initiation and values of 0.4% and 0.6% (by weight of binder) has been presented in BS EN 206 [2] and fib [36], respectively as an acceptable chloride threshold level (CTL). From the chloride profiles in Fig. 11, the chloride concentration at steel depth for both SCM concretes was 0.15% and 0.26% for CEM III/A and CEM II/B-V, respectively, which are lower than the tolerance value in the specifications. For the CEM I concrete, the chloride concentration was 0.8%; however, there were no visible signs of corrosion (e.g. rust staining, cracking). When compared to the data obtained from the field, the CTL specified in the code would appear to significantly underestimate the chloride concentration for corrosion initiation.

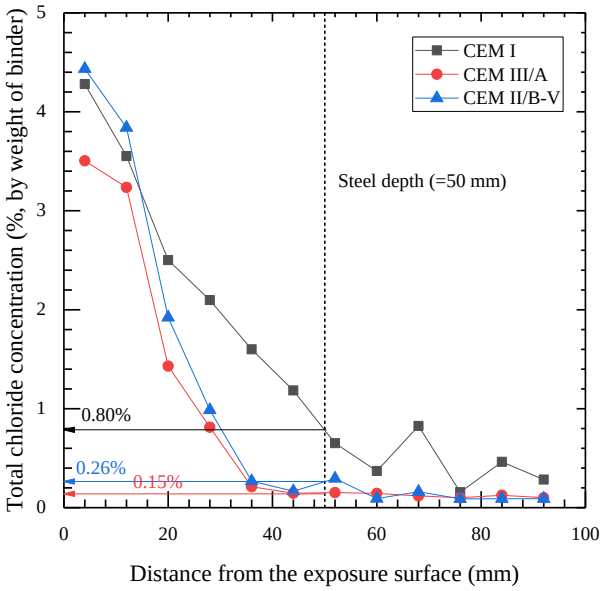

Fig. 11 Chloride profiles through slabs after 18 years exposure (XS3 environment)

4.2 Electrochemical Measurements on Embedded Steel

The products of corrosion result in cracking and spalling of the concrete cover which further accelerates the deterioration process. Although chloride ingress is a determinant in the corrosion of steel, it is still difficult to predict time to corrosion initiation as the CTL is not a

single value. To manage reinforced concrete structures subjected to chloride environments regular monitoring of the condition of steel is required. In this study, corrosion parameters including corrosion potential, ohmic resistance, polarisation resistance and *B* value were investigated together with half-cell potential, galvanostatic pulse technique and Tafel extrapolation technique. Figs. 12 and 13 show measured and fitting data in galvanostatic pulse and Tafel extrapolation measurements.

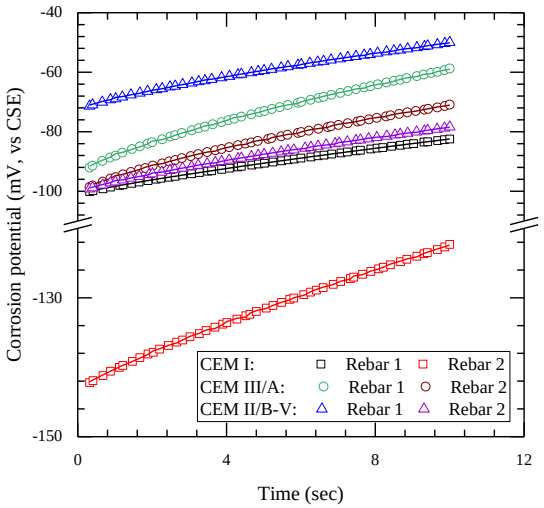

Fig. 12 Analysis of corrosion parameters in galvanostatic pulse technique (Solid line = Fitted line)

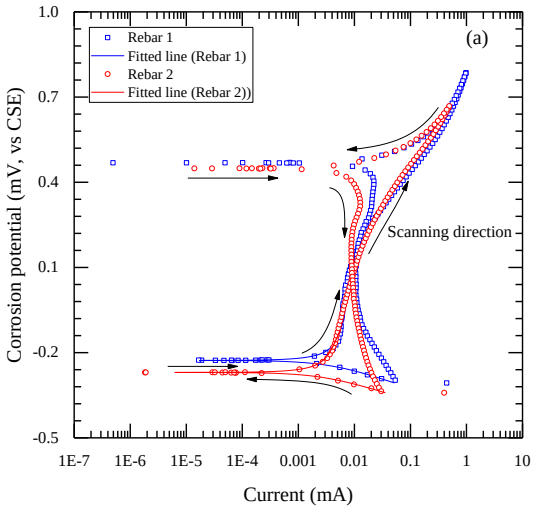

453

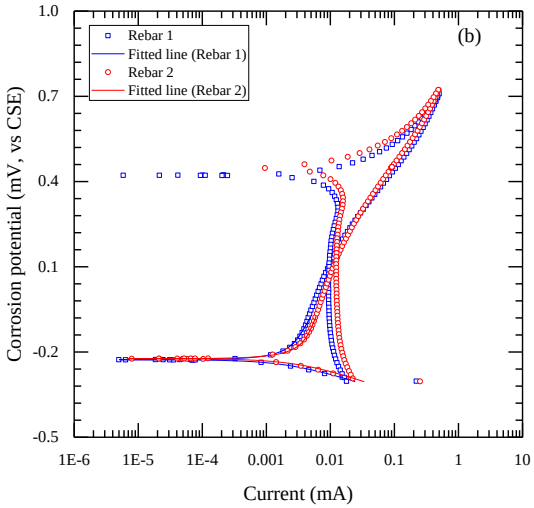

454

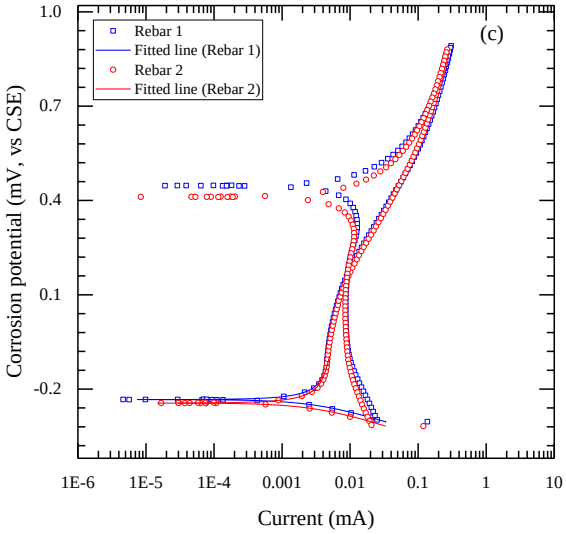

455 Fig .13. Measurements used for analysis of corrosion parameter (B value) in Tafel extrapolation
456 technique for (a) CEM I, (b) CEM III/A and (c) CEM II/B-V.

Table 3 presents the corrosion parameters for steel embedded in the slabs. Corrosion potential is widely used and according to ASTM C876 [37] the probability of corrosion is specified in Table. 4. Although the method is qualitative, all corrosion potentials were > -140mV (vs CSE), corresponding to a low probability of corrosion (<10%) in the specification. In order to quantify the corrosion rate, polarisation resistance and *B* values were evaluated. Although the rate is significantly lower in the passive state, the corrosion rates ranged from 2.2μA/m^2 to 6.3μA/m^2. Assuming that the corrosion rate ranges from 1 – 2 mA/m^2 at the onset of corrosion in concrete [38–41], the values presented were ~3 orders lower than the value required for the onset of corrosion. Hence, in the passive state, the corrosion rate is negligible.

The *B*-values obtained from the Tafel extrapolation method are similar to the value of 26mV which is normally recommended [42]. In the passive state, the *B*-value and polarisation resistance are minor factors in quantifying the corrosion rate; however, these values become critical after depassivation. Generally, the *B* value is set as 26mV in the active state, but can be widely distributed (2.2–86mV in the active state) [43–45]. The error caused by the *B*-value can be considerable. On the other hand, from the Tafel slopes, the corrosion activity was similar in a cathodic environment, irrespective of type of binder, as the samples were exposed to the same environment, i.e. XS3. The anodic reaction rate, however, varied with type of binder and steel rebar. Anodic slopes in the CEM II/B-V concrete were higher than those in the other concretes; hence, steel rebars embedded in CEM II/B-V concrete can have a better inhibition against corrosion. For CEM III/A concrete, the chloride concentration at steel depth (i.e. 50 mm) was lower than the CEM I concrete, but anodic slopes in both concretes ranged from 423.0 to 708.4mV/dec. It could be inferred that the CTL of CEM III/A concrete is lower than of CEM I concrete due to low buffering capacity in CEM III/A by a lower pH in pore solution.

In reinforced concrete, the ohmic resistance has an important influence on the corrosion rate and should be considered: CEM II/B-V concrete had the highest resistance followed by CEM III/A and CEM I concretes. Based on these measurements, CEM II/B-V concrete is the best binder in resisting chloride ingress and, once initiated, in slowing down the corrosion process.

	CEM I		CEM III/A		CEM II/B-V	
Steel Bar Number.	1	2	1	2	1	2
Ohmic resistance* (Ωm^2)	2.3	2.6	3.5	3.5	12.0	13.0
Polarisation resistance*(Ωm^2)	105.7	89.1	83.8	48.7	112.7	134.7
Corrosion potential (mV)	-99.8	-141.0	-94.8	-102.9	-96.2	-126.5
Time constant* (s)	212.1	142.7	84.7	48.9	226.8	293.7
Anodic slope** (mV/dec)	708.4	475.7	423.0	616.4	930.3	1082.9
Cathodic slope** (mV/dec)	70.2	62.9	71.0	79.1	72.2	70.7
B value (mV)	27.8	24.1	26.4	30.5	29.1	28.9
Corrosion current density ($\mu A/m^2$)	2.6	2.7	3.2	6.3	2.6	2.2

* Data obtained from Galvanostatic pulse technique
** Data obtained from Tafel slope

Table 3 Corrosion parameters of steel for samples at 18 years.

Potential (mV vs CSE)	Potential (mV vs Calomel electrode)	Probability of corrosion
>-200	>-126	Low (<10 %)
-200 - -350	-126 - -276	Intermediate
<-350	<-276	High (>90 %)

Table 4 Probability of corrosion from potential measurements [37].

4.3 Monitoring the Electrical Resistivity and Temperature of Field Concrete

The electrical resistivity is closely related to permeability/diffusivity of concrete according to the Nernst-Einstein equation [46]. The electrical resistivity of concrete is, on the other hand,

491 sensitive to both the ambient environment and material properties. Considering the age of
492 concrete used in this study, the influence of hydration on microstructure will be negligible;
493 however, other factors should be considered in evaluating concrete resistivity in the field
494 including temperature and degree of saturation and is developed below.

495 *4.3.1. The effect of temperature on the resistivity*

496 As conduction through concrete is, essentially, electrolytic in nature, it will be temperature
497 dependent. The influence of temperature on resistivity is linked through an Arrhenius
498 relationship [24] and, providing that the activation energy is known, the measured resistivity
499 can be *standardised* to an equivalent resistivity at a predefined reference temperature using
500 Eq. (10):

501 $$\rho_R = \rho_M e^{\frac{E_a}{R}\left[\frac{1}{T_{K,R}} - \frac{1}{T_{K,M}}\right]} \quad (10)$$

502 where ρ_R is the resistivity (Ωm) at the reference temperature; $T_{K,R}$ is the reference
503 temperature (=293.15K in this study) (K); ρ_M is the measured resistivity (Ωm) at
504 temperature, $T_{K,M}$ (K); R is the gas constant (8.314 J/mol·K); and E_a is the activation
505 energy for conduction processes in concrete (kJ/mol).

506 Fig 14(a) presents averaged ambient temperatures at discrete depths from the exposed surface
507 of the concrete slabs (error bars represent ± 1 standard deviation); over the time scale
508 presented, the temperature varied from 2.5ºC to 13.9ºC. From Fig. 14(b), it is evident that the
509 resistivity fluctuated in sympathy with the temperature – as the temperature increased, the
510 resistivity decreased and vice versa (note: in this Figure, for clarity, only the response from
511 10, 20, 30 and 40mm is presented).

512

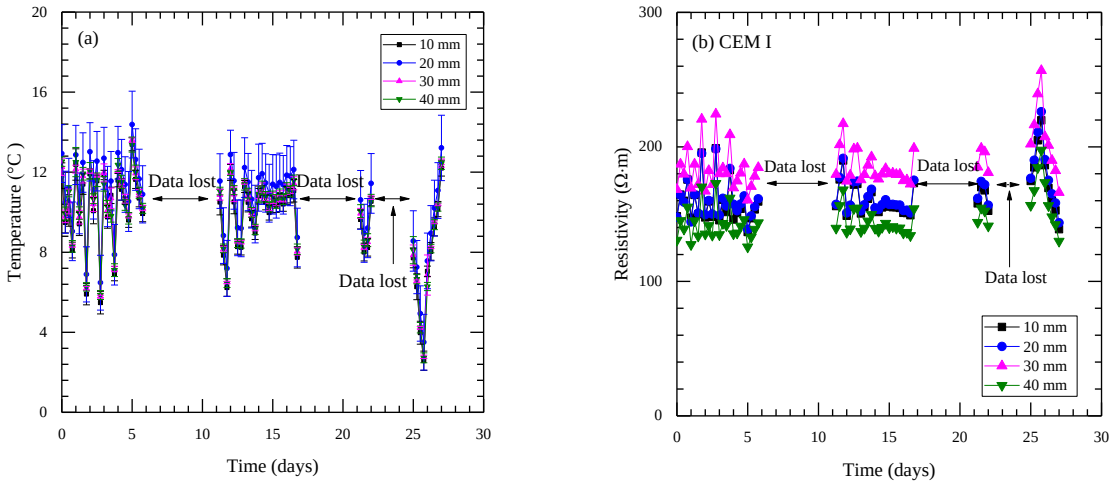

Fig. 14 Measurements obtained from remote monitoring of field concretes (XS3) showing the variation in (a) temperature and (b) electrical resistivity (CEM I concrete).

Fig. 15(a)-(c) presents the temperature/resistivity measurements in an Arrhenius format with the activation energy obtained from the slope of the straight line through the data; Fig. 16 presents the variation of activation energy with depth for each concrete type with the averaged values presented in the figure legend (27.94 kJ/mol for CEM I, 31.75 kJ/mol for CEM III/A and 30.46 kJ/mol for CEM II/B-V). Considering conduction occurs via capillary pore water, the low activation energy in CEM I concrete indicates a less tortuous and disconnected pore network compared to CEM III/A and CEM II/B-V concrete.

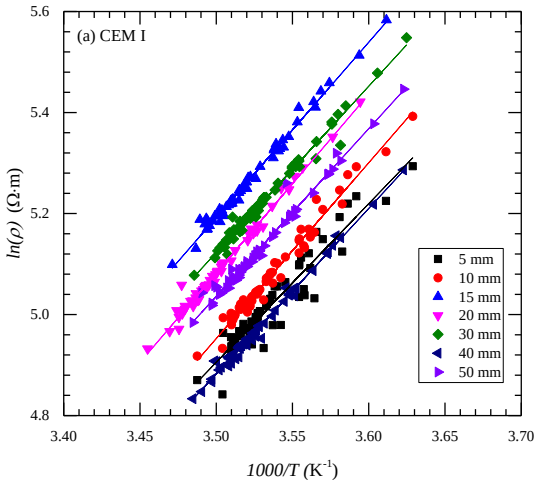

524

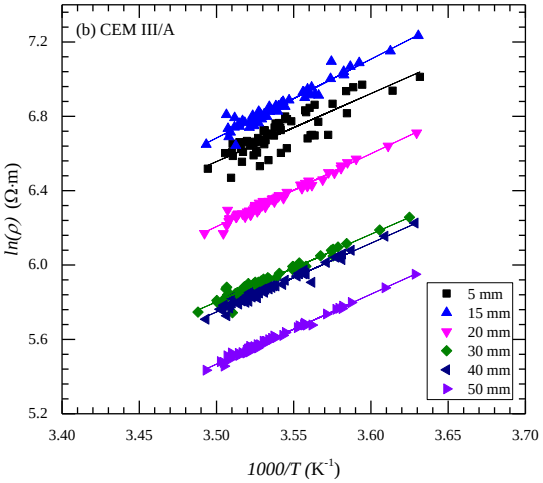

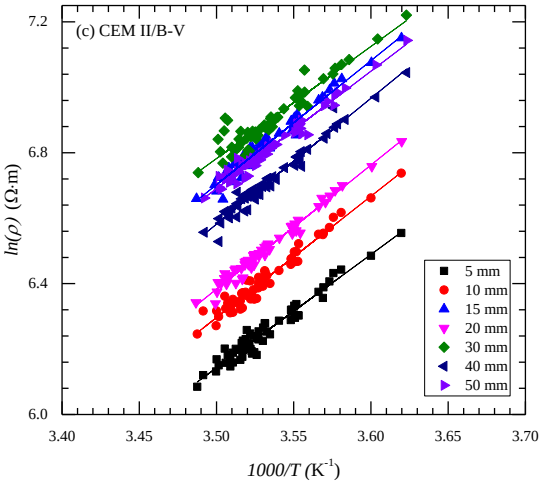

525
526 Fig 15. Field data plotted in Arrhenius format for (a) CEM I, (b) CEM III/A and (c) CEM II/B-V.
527 Note: data at 10mm on (b) was lost.
528
529
530

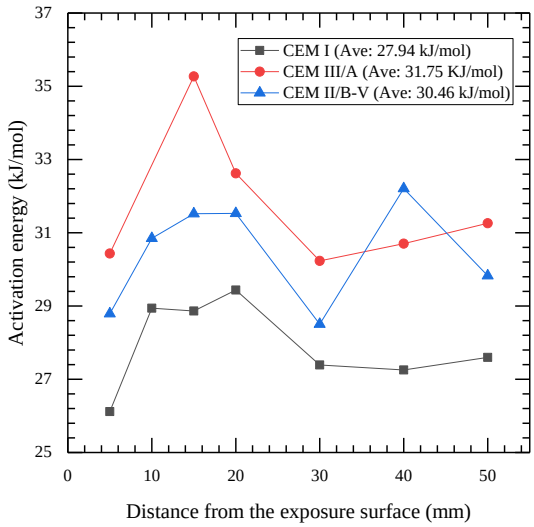

Fig. 16. Variation of activation energy with depth obtained from Fig. 15.

Fig. 17 shows the electrical resistivity of concrete after the correction using Eq. (10) and the average activation energy given above; the reference temperature was 20°C. During monitoring, some of the data were lost due to technical problems which remain unclear. It can be observed that the fluctuations in electrical resistivity observed in the uncorrected (i.e. raw) data become stable after the correction. As expected, CEM I concrete had the lowest resistivity; however, as the measured resistivity was > 100Ωm, irrespective of type of binder and depth, Table. 5 would indicate that all concretes could be regarded as offering good protection to the steel reinforcement [47].

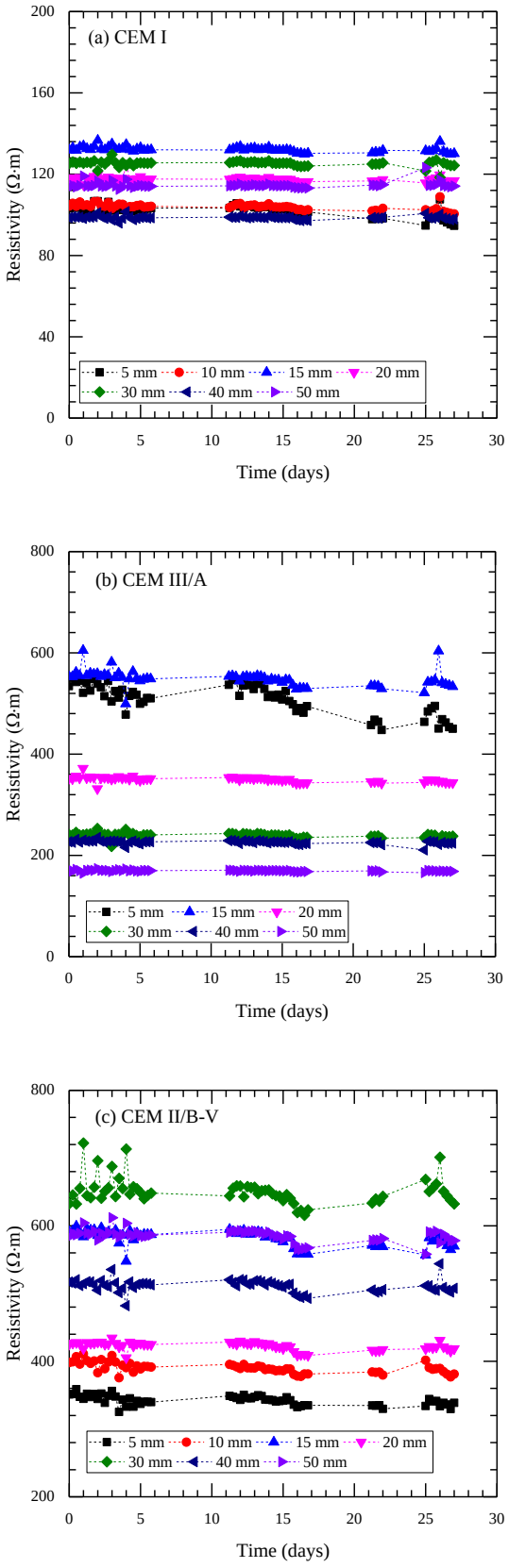

Fig. 17. Temperature corrected resistivity for (a) CEM I, (b) CEM III/A and (c) CEM II/B-V concretes. Note: data at 10mm on (b) were lost.

Resistivity (Ωm)	Probable Corrosion Rate
< 50	Very High
50 – 100	High
100 – 200	Moderate / low
> 200	Low

Table. 5 Empirical resistivity thresholds for protection of embedded steel reinforcement [47].

4.3.2 Prism and Field Resistivity Measurements

In this study, the resistivity of the prisms extracted from the slabs (i.e. the prisms used to measure degree of saturation in Section 3.1.2) was compared to the resistivity obtained from the slabs positioned at the marine exposure site using the remote interrogation facility. The results are presented in Fig. 18. It was observed that the resistivity of prisms in the vacuum-saturated condition is lower than the resistivity obtained from the embedded pins whilst the resistivity of the as-extracted prisms is similar to the resistivity of embedded pins. This result coincides with the result of degree of saturation. From the results, it could be inferred that the field concretes in the XS3 environment are in an unsaturated state under natural exposure. Again, considering that moisture movement is marginal, an increase in moisture content leads to an increase in chloride transport. It is interesting to note that the difference in the resistivity between the as-extracted prisms and vacuum-saturated prisms for the CEM II/B-V concrete is considerably greater than the other two concretes perhaps reflecting the lower degree of saturation of the as-extracted concrete prisms (see Fig. 10).

Finally, the electrical resistivity measurements using embedded pins, coupled with remote interrogation, is an attractive method for real-time monitoring of the long-term performance

564 of concrete in the field; however, further work is required to improve data acquisition in this
565 respect. Considering that the chloride concentration in SCM concretes at 50 mm depth is low,
566 the increase in resistivity may be caused by a continuous pozzolanic reaction. This is
567 beneficial to the performance of concrete and may also affect the resistivity of pore solution
568 in concrete which is one of the factors which determine the resistivity of concrete.

569

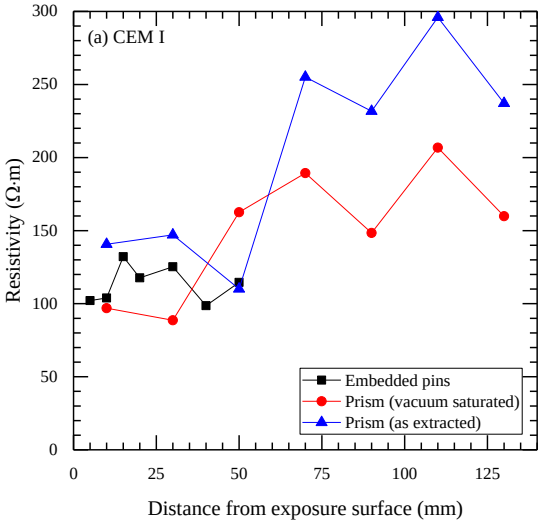

570

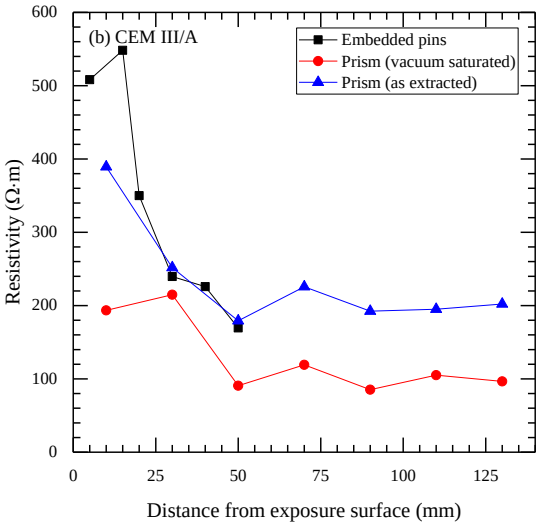

571

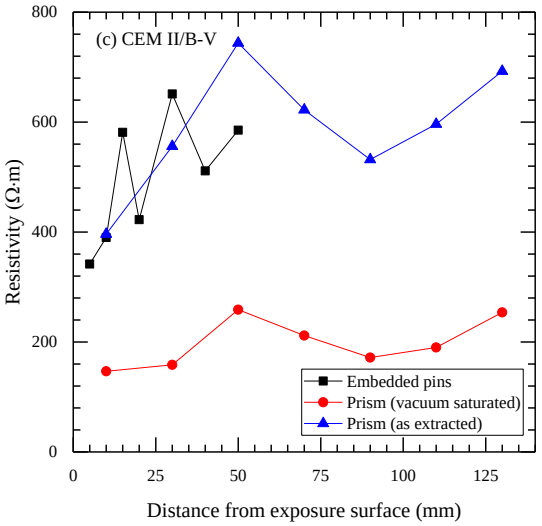

572
573 Fig. 18. Comparison of electrical resistivity of prisms (as-extracted and vacuum saturated conditions)
574 and embedded pins.
575

576 *4.4 Time to corrosion initiation considering environmental factors*

577 Prediction of the onset of corrosion in concrete was undertaken using the ClinConc model
578 [17]. This model describes chloride transport within concrete based on the principle of Fick's
579 law. The basic governing equation consists of the mass balance equation and a non-linear
580 chloride binding isotherm, as given by:

$$\frac{\partial q_{cl}}{\partial x} = -\frac{\partial}{\partial x}\left(D_0 \frac{\partial C_f}{\partial x}\right)$$

$$\frac{\partial C_t}{\partial t} = \frac{\partial C_f}{\partial t} + \frac{\partial C_b}{\partial t}$$

581 where, C_t, C_f and C_b are, respectively, the total, free and bound chloride concentrations,
582 q_{cl} is the net flux of free chloride per unit area and D_0 is the intrinsic diffusion coefficient.

583 The model input parameters include concrete mix proportions, binder type(s), curing and
584 environmental temperatures, the concentration of chloride in the solution to which a concrete
585 is exposed, and a 6-month chloride migration coefficient which needs to be obtained
586 experimentally from the non-steady migration test. Given that the ClinConc model is based
587 on diffusion, it is able to predict the chloride profile in concrete which, essentially, remains
588 fully saturated (i.e. completely submerged to seawater or below the mid-tide level). However,
589 it would be difficult to accurately determine an irregular boundary condition for concrete
590 exposed to tidal or splash zones where the concrete would be partially saturated and chloride
591 ingress due to direct contact with seawater tends to be random.

592 To take into account these aspects, two additional environmental factors have been
593 introduced [48]. From Fig. 10, the concretes used in this study were in an unsaturated state
594 (i.e. S_r <100%) and to reflect this condition, the environmental factors employed are:

(i) K_s which accounts for the reduction of diffusion coefficient with degree of saturation; and,

(ii) K_{exp} which accounts for the degree of contact of the concrete surface with the external *chloride* environment (i.e. tidal cycles).

The procedure for estimating the factors was as follows;

$$K_s = \frac{D_a}{D_0} = S_r^{4.863-3.441\frac{w}{b}} \quad (11)$$

$$C_t = K_{exp} \times \Phi(C_f) \quad (12)$$

where D_0 is the diffusion coefficient in saturated concrete; and D_a is the diffusion coefficient in the unsaturated concrete including the degree of saturation, S_r, and w/b is the water-to-binder ratio, C_t is total chloride content, Φ is the functional relationship defined within the ClinConc model [17] and C_f is free chloride content.

In formulating Eq. (11), the empirical relationship relating diffusion coefficient, degree of saturation and w/b has been adapted from the work of Kumar [49]. The ClinConc model requires the 6-month migration coefficient for the concrete as an input parameter obtained from the NT Build 492 test [27]. All the input parameters used in the ClinConc model are presented in Table 6. The mix specification was the same as that used in the 18-year old sample. K_s can be estimated from Eq. (11) and the averaged degree of saturation from Fig. 10 while K_{exp} values were found using the least square method between the measured and the predicted value. The details for the calculation procedure can be found in a previous study [48]. Fig. 19 presents the measured values and two predicted curves. One predicted curve is K_{exp} based on the best fitting for each type of concrete and the other is K_{exp} based on the averaged value for all three concrete mixes. As shown in the graphs, K_{exp} values are within a relatively narrow range 0.60-0.82 which is not surprising as the samples are in the same

exposure condition and have a similar w/b (0.39–0.44). In addition, the difference between two predicted curves was marginal when the average value for K_{exp} was used.

	CEM I	CEM III/A	CEM II/B-V
Cement content(kg/m^3)	460	270	370
Slag content(kg/m^3) (*k*-factor*)	+	180 (0.6)	+
Fly ash content (kg/m^3) (*k*-factor*)	+	+	160 (0.4)
Water content (l/m^3)	184	198	206.7
Average saturation degree	0.83	0.73	0.67
Average Temperature	9		
Concrete age at first exposure (days)	35		
Exposure duration (years)	18		
Chloride concentration applied at the surface (g/l)	19.6		
Migration coefficient at 6 months × 10^{-12} (m^2/s) (Standard deviation)	8.87 (±0.2)	3.33 (±0.5)	2.92 (±0.3)

* *k*-factor used in calculating equivalent binder content where the term 'w/b' is now w/(cement + k×SCM) defined in BS EN 206 [2]

Table. 6 Input parameters for the ClinConc model.

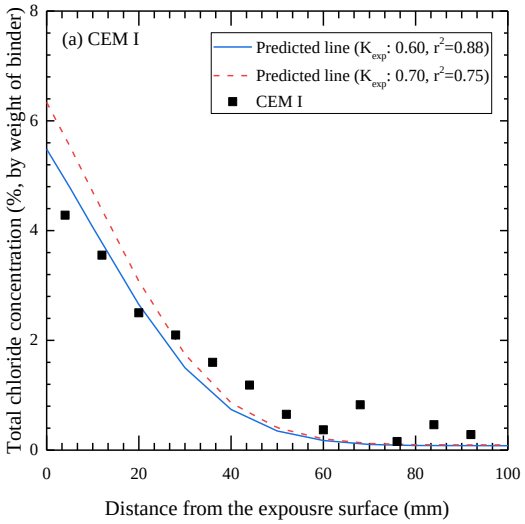

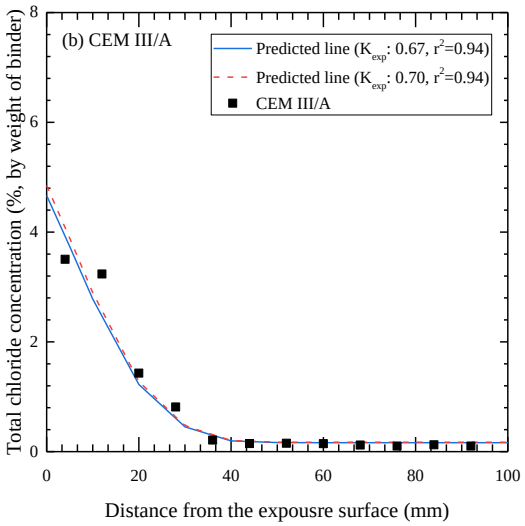

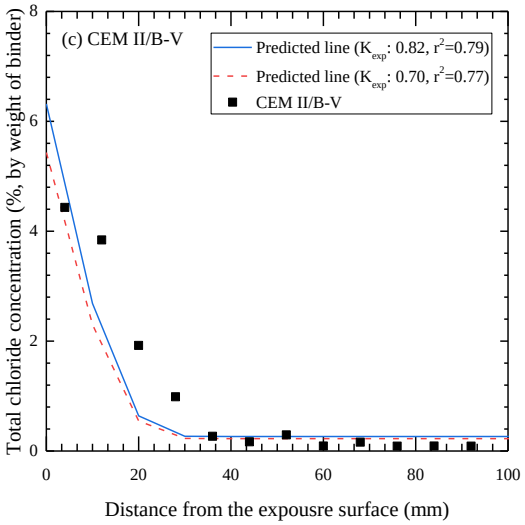

Fig. 19 Measured profile and predicted chloride profiles from the modified ClinConc model for (a) CEM I, (b) CEM III/A and (c) CEM II/B-V concrete subjected to XS3 environment.

The time to corrosion initiation was calculated with the average value as shown in Table. 7. CTLs can vary over the wide range, typically from 0.2% to 2.2%; hence, two CTLs were employed: 0.4% as the lower-bound value and 2.0% as upper-bound value. The time to attain the CTL at 50mm depth was highest for the CEM II/B-V concrete and increased by a factor of ~3.2 when the CTL increased from 0.4% to 2.0%. SCM concrete is thus beneficial in resisting chloride induced corrosion due to its low diffusivity. To increase the service-life of concrete structures subjected to marine environment, an increase in the acceptable CTL for the concrete can be an alternative as shown in the result; however, as the CTL is still controversial and is influenced by numerous factors [13, 14, 40] it is significantly difficult to control.

CTL*	Predicted time to corrosion initiation (year)		
	CEM I	CEM III/A	CEM II/B-V
0.4	17.8	49.8	114.3
2.0	55.6	179.5	342.5

* Chloride threshold level (% by weight of binder).

Table 7 The predicted time to attain the chloride threshold level at the steel depth.

5. CONCLUSIONS

In the current study, a comprehensive suite of tests was undertaken on concretes, with and without SCMs, subjected to a marine environment (XS3 exposure). As the concrete slabs were 18 years old, the data are representative of the performance of mature concrete, which is of importance in the development of performance-based specifications for concrete. The degree of saturation, porosity and chloride concentration were measured, together with their variation with depth from the concrete surface. Regarding the electrochemical condition of the steel, corrosion rate and half-cell potential were also evaluated. Based on chloride profiles,

645 the service life of reinforced concrete was predicted using the ClinConc model combined
646 with two environmental factors to take account for concrete in an unsaturated state and cyclic
647 exposure to chlorides. The following general conclusions can be drawn from the work:

648 (1) Regarding the degree of saturation and diffusion coefficient, CEM I concrete had the
649 highest, but the porosity of CEM I concrete was the lowest. To evaluate the resistance
650 of chloride transport in reinforced concrete, pore structure, i.e. tortuosity and
651 connectivity, should be considered rather than overall porosity. It was confirmed that
652 SCMs concretes were beneficial to resist chloride transport due to disconnected pore
653 structure caused by continuous hydration and high chloride binding.

654 (2) Although the chloride concentration at steel depth was 0.8% by weight of binder for
655 CEM I concrete, corrosion of steel was not detected. Corrosion potentials for all
656 concretes were > -140mV vs CSE corresponding to <10 % in probability of corrosion
657 as specified in ASTM C876. The *B*-values ranged from 24.1 to 30.5mV irrespective
658 of type of binder. It is considered that a low *B*-value resulted from high availability of
659 oxygen as concretes were exposed to the tidal and splash zones.

660 (3) To reflect the effect of temperature on electrical resistivity, the activation energy was
661 evaluated with the field concrete. It was observed that the activation energy varied
662 with depth and type of binder, ranging from 27.94 to 31.75kJ/mol. It was confirmed
663 that the activation energy was also influenced by contamination of chloride and
664 moisture-content. Depending on type of chlorides present in concrete (i.e. free/bound),
665 the electrical resistivity, especially in the surface region, increased or decreased.

666 (4) The electrical resistivity of all concretes was > 100 Ωm, indicating that the probability
667 of chloride-induced corrosion of steel in the reinforced concrete is low. From

comparison of resistivity between prisms and field samples, all concretes were in an unsaturated state in their natural condition. In addition, it was confirmed that moisture movement is marginal from the stable values in the resistivity, irrespective of depth and binder type although field concretes investigated in this study were exposed to tidal action.

Evaluating the long-term performance of concrete in the field yields valuable information as the data reflect both exposure condition and material properties. As the exposure condition cannot be exactly simulated within a laboratory environment, field monitoring assumes even greater significance. Electrical resistivity represents an important candidate testing methodology for non-destructive (and real-time) monitoring of the performance of as-placed concrete and warrants further development.

ACKNOWLEDGEMENT

The Authors wish to thank Professor Malcolm Chrisp (Head of School) for placing the facilities of the School at their disposal.

683 **REFERENCES**

684 [1] A.E.K. Jones, B. Marsh, L. Clark, D. Seymour, P. Basheer, A. Long A, BCA Research
685 Report C/21, Development of a holistic approach to ensure the durability of new
686 concrete construction, British Cement Association, Camberley, UK, 1997.

687 [2] British Standards Institution, BS EN 206 Concrete — Specification, performance,
688 production and conformity, British Standards Institution, London, 2014.

689 [3] U. M. Angst, R. D. Hooton, J. Marchand, C. L. Page, R. J. Flatt, B. Elsener, C. Gehlen,
690 J. Gulikers, Present and future durability challenges for reinforced concrete structures,
691 Mater. Corros. 63 (2012), 1047-1051. doi:10.1002/maco.201206898

692 [4] British Standards Institution, BS 8500-1+A1 Concrete-Complementary British
693 Standard to BS EN 206 — Part 1: Method of specifying and guidance for the specifier,
694 British Standards Institution, London, 2016.

695 [5] ACI Committee 318, Building code requirements for structural concrete (ACI 318-14)
696 and commentary on building code requirements for structural concrete (ACI 318R-14),
697 American Concrete Institute, Michigan, 2014

698 [6] J.G. Kessy, M.G. Alexander, H. Beushausen, Concrete durability standards:
699 International trends and the South African context, J. S. Afr. Instr. Civ. Eng. 57 (2015)
700 47-58.

701 [7] Japan Society of Civil Engineers, Standard specifications for concrete structure-2007
702 'Design', Japan Society of Civil Engineers, Tokyo, 2010.

703 [8] Japan Society of Civil Engineers, Standard specifications for concrete structure-2007
704 'Materials and Construction', Japan Society of Civil Engineers, Tokyo, 2010.

705 [9] V. Baroghel-Bouny, M. Thiéry, X. Wang, Performance-based assessment of durability
706 and prediction of RC structure service life: transport properties as input data for
707 physical models, Mater. Struct. 47 (2014) 1669–1691. doi:10.1617/s11527-013-0144-z.

708 [10] P.B. Bamforth, W.F. Price, M. Emerson, An international review of chloride ingress
709 into structural concrete, Transport Research Laboratory, Wokingham, 1997. ISBN 0-
710 7277-2928-4.

711 [11] M.D.A. Thomas, P.B. Bamforth, Modelling chloride diffusion in concrete effect of fly
712 ash and slag, Cem. Concr. Res. 29 (1999) 487–495. doi:10.1016/S0008-
713 8846(98)00192-6.

714 [12] J. Zuquan, Z. Xia, Z. Tiejun, L. Jianqing, Chloride ions transportation behavior and
715 binding capacity of concrete exposed to different marine corrosion zones, Constr.
716 Build. Mater. 177 (2018) 170-183. doi.org/10.1016/j.conbuildmat.2018.05.120.

717 [13] U. Angst, B. Elsener, C.K. Larsen, Ø. Vennesland, Critical chloride content in
718 reinforced concrete - A review, Cem. Concr. Res. 39 (2009) 1122–1138.
719 doi:10.1016/j.cemconres.2009.08.006.

720 [14] G.K. Glass, N.R. Buenfeld, The presentation of the chloride threshold level for
721 corrosion of steel in concrete, Corros. Sci. 39 (1997) 1001–1013. doi:10.1016/S0010-
722 938X(97)00009-7.

[15] R.E. Melchers, I.A. Chaves, A comparative study of chlorides and longer-term reinforcement corrosion, Mater. Corros. 68 (2017) 613-621. doi: 10.1002/maco.201609310

[16] R.B. Polder. Critical chloride content for reinforced concrete and its relationship to concrete resistivity, Mater. Corros. 60 (2009) 623-630. doi:10.1002/maco.200905302

[17] L. Tang, Engineering expression of the ClinConc model for prediction of free and total chloride ingress in submerged marine concrete, Cem. Concr. Res. 38 (2008) 1092–1097. doi:10.1016/j.cemconres.2008.03.008.

[18] L. Tang, P. Utgenannt, A field study of critical chloride content in reinforced concrete with blended binder, Mater. Corros. 60 (2009) 617-622. doi:10.1002/maco.200905282.

[19] M.D.A. Thomas, J.D. Matthews, Performance of pfa concrete in a marine environment-10-years results, Cem. Concr. Compos. 26 (2004) 5-20. doi: 10.1016/S0958-9465(02)00117-8.

[20] M. Otieno, H. Beushausen, M. Alexander, Chloride-induced corrosion of steel in cracked concrete-Part I: Experimental studies under accelerated and natural marine environments, Cem. Concr. Res. 79 (2016) 373-385. doi: 10.1016/j.cemconres.2015.08.009.

[21] M.D.A Thomas, T. Bremner, Performance of lightweight aggregate concrete containing slag after 25 years in a harsh marine environment, Cem. Concr. Res. 42 (2012) 358-364. doi: 10.1016/j.cemconres.2011.10.009.

[22] W.J. McCarter, T.M. Chrisp, G. Starrs, P.A.M. Basheer, J. Blewett, Field monitoring of electrical conductivity of cover-zone concrete, Cem. Concr. Compos. 27 (2005) 809-817. doi: 10.1016/j.cemconres.2011.10.009.

[23] W. Morris, A. Vico, M. Vazquez, Chloride induced corrosion of reinforcing steel evaluated by concrete resistivity measurements, Electrochim. Acta. 49 (2004) 4447-4453. doi:10.1016/j.electacta.2004.05.001.

[24] W.J. McCarter, T.M. Chrisp, G. Starrs, A. Adamson, E. Owens, P.A.M. Basheer, S.V. Nanukuttan, S. Srinivasan, N. Holmes, Developments in performance monitoring of concrete exposed to extreme environments, J. Infrastruct. Syst. 18 (2012) 167–175. doi:10.1061/(ASCE)IS.1943-555X.0000089.

[25] W.J. McCarter, M. Emerson, H. Ezirim, Properties of concrete in the cover zone: developments in monitoring techniques, Mag. Concr. Res. 47 (1995) 243–251.

[26] British Standards Institution, PD CEN/TR 16563 Principles of the equivalent durability procedure, British Standards Institution, London, 2013.

[27] Nordtest, NT Build 492 Concrete, mortar and cement-based repair materials: Chloride migration coefficient from non-steady-state migration experiments, Nordtest, Espoo, 1999.

[28] N. Birbilis, K.M. Nairn, M. Forsyth, On the electrochemical response and interfacial properties of steel-$Ca(OH)_2$ and the steel-concrete system measured using galvanostatic pulses, Electrochim. Acta. 49 (2004) 4331–4339. doi:10.1016/j.electacta.2004.03.042.

[29] BETATHERM NTC-THERMISTOR, BetaTHERM Sensors-NTC Thermistor theory, http://beta.dk/wp-content/uploads/2014/11/teoridel.pdf, 2014 (accessed April 26, 2018).

[30] W.J. McCarter, G. Starrs, A. Adamson, T.M. Chrisp, P.A.M. Basheer, S.V. Nanukuttan, S. Srinivasan, C. Green, Influence of different european cements on the hydration of cover-zone concrete during the curing and postcuring periods, J. Mater. Civ. Eng. 25 (2013) 1335–1343. doi:doi:10.1061/(ASCE)MT.1943-5533.0000678.

[31] S. Li, D.M. Roy, Investigation of relations between porosity, pore structure, and C1− diffusion of fly ash and blended cement pastes, Cem. Concr. Res. 16 (1986) 749–759. doi:https://doi.org/10.1016/0008-8846(86)90049-9.

[32] S. Lu, E.N. Landis, D.T. Keane, X-ray microtomographic studies of pore structure and permeability in Portland cement concrete, Mater. Struct. 39 (2006) 611–620. doi:10.1617/s11527-006-9099-7.

[33] Y.H. Gao, J.Z. Zhang, S. Zhang, Y.R. Zhang, Probability distribution of convection zone depth of chloride in concrete in a marine tidal environment, Constr. Build. Mater. 140 (2017) 485–495. doi:10.1016/j.conbuildmat.2017.02.134.

[34] L. Tang, SP Report 2003:16, Chloride ingress in concrete exposed to marine environment: Field data up to 10 years exposure, SP Swedish National Testing and Research Institute, Boras, Sweden, 2003.

[35] H.W. Song, C.H. Lee, K.Y. Ann, Factors influencing chloride transport in concrete structures exposed to marine environments, Cem. Concr. Compos. 30 (2008) 113-121. doi:10.1016/j.cemconcomp.2007.09.005.

[36] fib, Bulletin no. 34, Model code for service life design, The International Federation for Structural Concrete, Lausanne, Switzerland, 2006.

[37] ASTM International, ASTM C876 Standard test method for corrosion potentials of uncoated reinforcing steel in concrete, ASTM International, West Conshohocken, Pennsylvania, 2015.

[38] K.Y. Ann, T.S. Kim, J.H. Kim, S.H. Kim, The resistance of high alumina cement against corrosion of steel in concrete, Constr. Build. Mater. 24 (2010) 1502–1510. doi:10.1016/j.conbuildmat.2010.01.022.

[39] I. Martinez, F. Rozas, S. Ramos-Cillan, M. González, M. Castellote, Chloride Electroremediation in reinforced structures: Preliminary electrochemical tests to detect the steel repassivation during the treatment, Electrochim. Acta. 181 (2015) 288–300. doi:10.1016/j.electacta.2015.06.005.

[40] C. Alonso, M. Castellote, C. Andrade, Chloride threshold dependence of pitting potential of reinforcements, Electrochim. Acta. 47 (2002) 3469–3481. doi:10.1016/S0013-4686(02)00283-9.

[41] M.J. Jung, K.B. Kim, S.A. Lee, K.Y. Ann, Risk of chloride-induced corrosion of steel in SF concrete exposed to chloride-bearing environment, Constr. Build. Mater. 166 (2018) 413-422. doi.org/10.1016/j.conbuildmat.2018.01.168.

[42] RILEM TC 154-EMC, Test methods for on-site corrosion rate measurement of steel reinforcement in concrete by means of the polarization resistance method, Mater. Struct. 37 (2004) 623–643. doi:10.1617/13952.

[43] G. Song, Theoretical analysis of the measurement of polarisation resistance in reinforced concrete, Cem. Concr. Compos. 22 (2000) 407–415. doi:10.1016/S0958-9465(00)00040-8.

[44] Z.T. Chang, B. Cherry, M. Marosszeky, Polarisation behaviour of steel bar samples in concrete in seawater. Part 2: A polarisation model for corrosion evaluation of steel in concrete, Corros. Sci. 50 (2008) 3078–3086. doi:10.1016/j.corsci.2008.08.021.

[45] A. Michel, M. Otieno, H. Stang, M.R. Geiker, Propagation of steel corrosion in concrete: Experimental and numerical investigations, Cem. Concr. Compos. 70 (2016) 171–182. doi:10.1016/j.cemconcomp.2016.04.007.

[46] W.J. McCarter, T.M. Chrisp, G. Starrs, P.A.M. Basheer, S.V. Nanukuttan, S. Srinivasan, B.J. Magee, A durability performance-index for concrete: developments in a novel test method, Int. J. Struct. Eng. 6 (2015) 2-22. doi:10.1504/IJSTRUCTE.2015.067966.

[47] J.P. Broomfield, Corrosion of steel in concrete, first ed., E&FN Spon, London, 1997. ISBN 0-491-19630-7.

[48] J. Kim, W.J. McCarter, B. Suryanto, S. Nanukuttan, P.A.M. Basheer, T.M. Chrisp, Chloride ingress into marine exposed concrete: A comparison of empirical- and physically- based models, Cem. Concr. Compos. 72 (2016) 133–145. doi:10.1016/j.cemconcomp.2016.06.002.

[49] A. Kumar, Water flow and transport of chloride in unsaturated concrete, MSc, University of Saskatchewan, 2010.